JACS
JOURNAL OF THE AMERICAN CHEMICAL SOCIETY
pubs.acs.org/JACS
Article

Quantum Dot-Sensitized Photoreduction of CO_2 in Water with Turnover Number > 80,000

Francesca Arcudi,[¶] Luka Đorđević,[¶] Benjamin Nagasing, Samuel I. Stupp, and Emily A. Weiss*

Cite This: *J. Am. Chem. Soc.* 2021, 143, 18131−18138
Read Online

ABSTRACT: Climate change and global energy demands motivate the search for sustainable transformations of carbon dioxide (CO_2) to storable liquid fuels. Photocatalysis is a pathway for direct conversion of CO_2 to CO, one step within light-powered reaction networks that could, if efficient enough, transform the solar energy conversion landscape. To date, the best performing photocatalytic CO_2 reduction systems operate in nonaqueous solvents, but technologically viable solar fuels networks will likely operate in water. Here we demonstrate catalytic photoreduction of CO_2 to CO in pure water at pH 6−7 with an unprecedented combination of performance parameters: turnover number (TON-(CO)) = 72,484−84,101, quantum yield (QY) = 0.96−3.39%, and selectivity (S_{CO}) > 99%, using $CuInS_2$ colloidal quantum dots (QDs) as photosensitizers and a Co-porphyrin catalyst. At higher catalyst concentration, the system reaches QY = 3.53−5.23%. The performance of the QD-driven system greatly exceeds that of the benchmark aqueous system (926 turnovers with a quantum yield of 0.81% and selectivity of 82%), due primarily to (i) electrostatic attraction of the QD to the catalyst, which promotes fast multielectron delivery and colocalization of protons, CO_2, and catalyst at the source of photoelectrons, and (ii) termination of the QD's ligand shell with free amines, which capture CO_2 as carbamic acid that serves as a reservoir for CO_2, effectively increasing its solubility in water, and lowers the onset potential for catalytic CO_2 reduction by the Co-porphyrin. The breakthrough efficiency achieved in this work represents a nonincremental step in the realization of reaction networks for direct solar-to-fuel conversion.

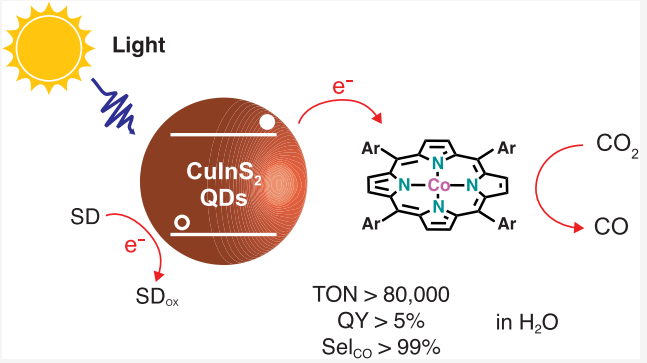

INTRODUCTION

Solar energy is by far the largest source of clean, renewable energy for sustainable, carbon-neutral fuel production.[1−5] Direct solar-to-fuels systems, which colocalize the functions of light absorption, charge separation, and redox-driven chemistry, have emerged as an alternative to photovoltaic-driven electrochemical cells because they avoid the fabrication processes associated with Si (or other efficient) solar cells and can, in principle, be designed to access a greater variety of chemical products useful for fuel and agriculture.[6−14] Photocatalytic systems for direct production of CO from CO_2 are expected to play a major part in solar fuels cascade networks, but the best-performing systems are still far from technologically relevant targets.[15−21]

High-turnover, robust, selective systems for conversion of CO_2 to CO have been realized in organic solvents or partially aqueous media (Table S1, Supporting Information (SI)).[22−27] In most cases, these systems comprise electrocatalysts capable of driving CO_2 reduction in combination with photosensitizers—typically based on expensive metals such as ruthenium or iridium—that absorb light and donate electrons to the catalyst. This previous work represents an important advance, but the opportunity to source electrons for CO_2 reduction from water oxidation, plus the abundance and zero environmental impact of water, strongly motivates the development of photocatalytic reactions that operate in *pure* water. Fully aqueous photocatalytic reduction of CO_2 must however overcome (i) a low selectivity for carbonaceous products[28] due to kinetically and thermodynamically favored proton reduction and (ii) the poor solubility of CO_2 in water ($[CO_2]$ = 0.0383 M at 298 K under 1 atm).[29] There are few encouraging reports of aqueous photocatalytic CO_2 reduction,[30−36] but the performance of these systems severely lags that of analogous nonaqueous systems (Table S1, SI). Furthermore, a CO-evolution system that simultaneously performs well with respect to all three key metrics—turnover number (TON), quantum yield (QY), and selectivity (S_{CO})—has proven challenging both in organic solvents and in aqueous media (Table S1, SI). For example, a Ni-complex/$Ir(ppy)_3$ system achieved a TON of 98,000, and an S_{CO} close to 1 in

Received: July 5, 2021
Published: October 19, 2021

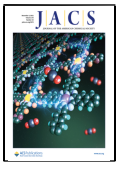

https://doi.org/10.1021/jacs.1c06961
J. Am. Chem. Soc. 2021, 143, 18131−18138

acetonitrile, but with a QY of 0.01%.[25] A dinuclear metal catalyst achieved a TON of 65,000 (S_{CO} = 0.98) in water/acetonitrile (1:4, v/v), but with a QY of 0.15%.[24] The CO dehydrogenase enzyme sensitized by CdS nanorods yielded a TON of 22,500 in aqueous buffer, but the QY was only 0.01%.[34] Similarly, the best QYs have been achieved using systems with low TON and selectivity. The QY of a Re system in dimethylformamide was 74%, but with only 48 TONs.[37] A Ru system produced a QY of 11.6% in *N*,*N*-dimethylacetamide/water (9:1, v/v), but the TON was only 164 with S_{CO} = 0.59.[26] A Ru−Re system achieved a QY of 13.5% in water, but with a TON of only 130 and S_{CO} = 0.81.[38]

Here we report a colloidal photocatalytic system—heavy metal-free $CuInS_2$/ZnS core/shell colloidal quantum dots (QDs) as photosensitizers for a [{*meso*-tetra(4-sulfonatophenyl)porphyrinato}cobalt(III)] (CoTPPS) catalyst, Figure 1—that converts CO_2 to CO in pure water (pH = 6−7) with unprecedented performance along all three key dimensions simultaneously: TON > 80,000, S_{CO} > 99%, and QY = 5.2%, plus a sensitization efficiency (ξ = molecules of CO produced per J of absorbed photon energy) of 95.8. The best-performing system reported in the literature, which uses the same CoTPPS catalyst with a $[Ru(bpy)_3]^{2+}$ photosensitizer, yielded TON = 926, S_{CO} = 82%, QY = 0.81%, and ξ = 9.3.[35]

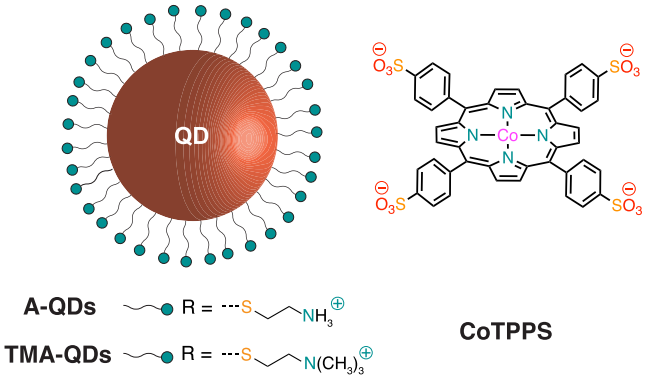

Figure 1. Structure of sensitizer and catalyst. $CuInS_2$/ZnS core/shell QDs capped with 2-aminoethanethiol hydrochloride (A-QDs) or 2-mercaptoethyl-*N*,*N*,*N*-trimethylammonium chloride (TMA-QDs), [{*meso*-tetra(4-sulfonatophenyl)porphyrinato}cobalt(III)] (CoTPPS).

We knew from previous work on $CuInS_2$ QD-Fe porphyrin systems that the large extinction coefficient (~70,000 $M^{-1}\cdot cm^{-1}$ at 450 nm, roughly 5× greater than that of $[Ru(bpy)_3]^{2+}$) and high reduction potential (between −1.9 V and −2.4 V vs SCE)[39,40] of these QDs make them excellent sources of multiple photoelectrons for porphyrins,[39] especially when the QDs and porphyrins are functionalized to form colloidally stable electrostatic assemblies in water.[41] The quasi-static donor−acceptor complexes within these assemblies increase the rate constant for charge transfer from the QDs to the porphyrin. Additionally, we can terminate the ligands on the surfaces of QDs in groups known to capture and preactivate CO_2.[42−45] We therefore synthesized QDs coated in ligands terminated with amines/ammoniums (A-QDs) or, for comparison, trimethylammoniums (TMA-QDs), and mixed these positively charged QDs with negatively charged CoTPPS, Figure 1. We hypothesized that both the A-QDs and TMA-QDs would couple electrostatically to CoTPPS, but only the A-QDs would capture the CO_2,[46−48] as carbamic acid, and thereby enhance the catalytic activity of CoTPPS and suppress the competing hydrogen evolution reaction.[43,44,49,50]

RESULTS AND DISCUSSION

Performance of the QD-CoTPPS System for Photocatalytic Reduction of CO_2 to CO in Pure Water. Each photocatalytic reaction mixture in pure water contained a sensitizer (A-QDs, TMA-QDs, or, for comparison to the best-performing system,[35] $[Ru(bpy)_3]^{2+}$); the catalyst CoTPPS; and sodium ascorbate (NaAsc) as the sacrificial reductant. In a typical run, we illuminated a catalytic mixture in 2.0 mL of water under 1 atm of CO_2 using a 450 nm light-emitting diode (LED); the Supporting Information (SI) contains details of the photocatalytic setup. Reaction mixtures without QDs yielded no photoreduction products; trace H_2 (18.5 nmol) was detected in the absence of CoTPPS (Table S2, SI). Before bubbling CO_2, the pH of the reaction mixture was between 6 and 7, and the catalytic activity was not dependent on the pH in this range, Table S2 (SI). Others have optimized CO_2 reduction systems by adjusting the pH with addition of salts, but addition of $NaHCO_3$, which served as a pH buffer in the best reported system,[35,51] always decreased the activity of our system (Table S2, SI) probably by deprotonating the terminal amines and thereby destabilizing the colloidal suspension. Figure S1 (SI) summarizes our extensive optimization of this system with respect to concentrations of sensitizer, catalyst, and NaAsc. Under the tentatively optimal composition of the reaction mixture of 2.5 μM A-QDs, 0.25 μM CoTPPS, and 25 mM NaAsc, an 18 h illumination produced CO with TON = 50,017 and S_{CO} = 99.1% over H_2 evolution with a maximum TOF = 4,114 h^{-1} (Figure S2, SI). Analysis of the liquid phase by ^1H NMR detected no other products.

Figure 2a shows the generation of CO by the optimized systems containing A- and TMA-QDs as a function of irradiation time. A-QDs and TMA-QDs produced CO selectively (99%) with a TON (quantum yield, QY) of 72,494 (3.39%) and 38,473 (0.53%), respectively (Table 1, entries 1 and 5; Figure 2a−b). We improved the QY for the photocatalytic production of CO to 5.2% by increasing the concentration of CoTPPS from 0.25 μM to 2.5 μM for the system containing A-QDs, with the selectivity for CO over H_2 remaining > 99% (Table 1, entry 2 and Figure S3, SI). Further increase of the CoTPPS concentration will likely result in its parasitic light absorption by the catalyst (Figures S8−S9, SI). Our QY of 5.2% with single-wavelength excitation is among the highest reported to date for CO production in water (Table S1, SI).

When we use a combination of tris(carboxyethyl)phosphine (TCEP) and NaAsc as a sacrificial donor, the TON for CO further increases to 84,101 while maintaining a selectivity of >99% with a maximum TOF = 8,063 h^{-1} (Table 1, entry 3; Figure 2a−b, and Figure S2, SI). TCEP is known to continuously reduce the dehydroascorbic acid (DHA) to NaAsc[52] and thereby suppress inhibition of photocatalysis by DHA.[52] The data in Figures S4 and S5 and Table S2 (SI) confirm that readdition of the initial amount of QDs restores catalysis (more so than does the readdition of the initial amount of CoTPPS or of NaAsc), and that accumulation of DHA during prolonged illumination of the reaction mixture, or direct addition of DHA to the reaction mixture, encourages precipitation of the QDs and halts catalysis. In the absence of a sacrificial donor, the A-QDs-CoTPPS system yields CO

https://doi.org/10.1021/jacs.1c06961
J. Am. Chem. Soc. 2021, 143, 18131−18138

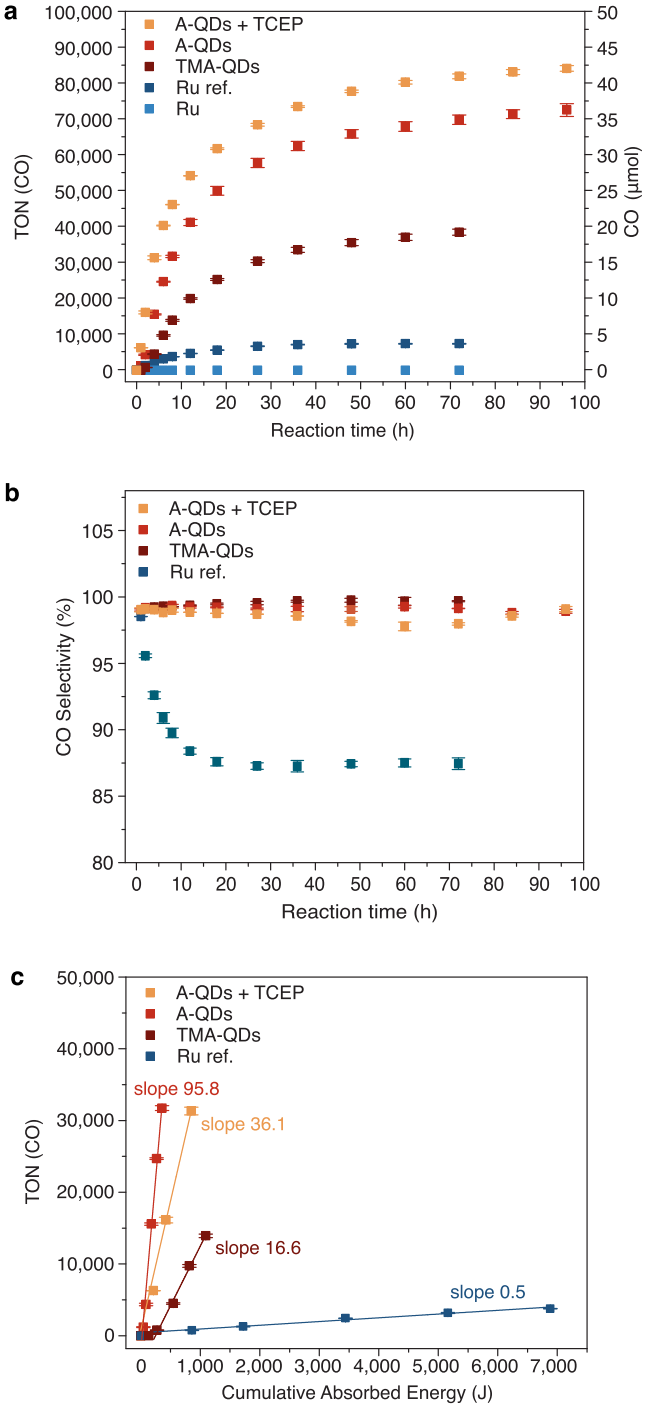

Figure 2. Catalytic performance metrics. (a) Concentration of CO and (b) selectivity for CO as a function of time of irradiation (450 nm, 140 mW·cm^{-2}) for samples prepared in 2.0 mL of CO_2-saturated H_2O. (c) Plot of TON (CO) vs the cumulative absorbed photon energy (slope = sensitization efficiency). Error bars are calculated from two to three runs; uncertainty is ≤5%. Table 1 details the compositions of all samples. The "Ru" sample contains 12 μM of sensitizer (a concentration that matches the absorbance of the QDs samples at 450 nm). The "Ru ref." sample has a composition optimized in ref 35.

selectively, with a TON of 2,394 after 18 h (Table S2, SI). NMR spectra of the catalytic mixture before irradiation include two triplets corresponding to the excess ligand (2-aminoethanethiol) (Figure S6, SI). After irradiation, two new triplet peaks appear, attributable to the oxidized form of the ligand, 2,2′-diaminodiethyl disulfide (Figure S6, SI). When excess ligand is not present, the same catalytic system yielded no CO (Table S2, SI). These results show that aminoethanethiol acts as the primary hole scavenger in the absence of ascorbate.[53]

Photocatalytic experiments for the A-QD-CoTPPS system were repeated on samples that underwent three freeze–pump–thaw (FPT) cycles (completely removing all CO_2 from the system) before bubbling either $^{13}CO_2$ or CO_2. GC-MS analysis of product shows that peaks from CO and ^{13}CO are exchanged when CO_2 substrate was switched to $^{13}CO_2$ (Figures 3a–b and Figure S7, SI), providing an unambiguous confirmation that CO originates from CO_2 reduction.[54]

The optimized QY of our A-QD system (QY = 5.2%) is a factor of 6.4 higher than the optimized value in the benchmark report, which uses a combination of a $[Ru(bpy)_3]^{2+}$ sensitizer and the CoTPPS catalyst.[35] The optimized TON of our A-QD system (TON = 84,101 with S_{CO} = 99%) is a factor of 91 higher than the optimized value in the benchmark report (TON = 926 with S_{CO} = 82%),[35] even though the concentration of QDs is a factor of 200 lower than that of $[Ru(bpy)_3]^{2+}$.

In the $[Ru(bpy)_3]^{2+}$-CoTPPS system, the TON is sensitive to catalyst concentration: the TON increases from 926 to *ca.* 4,000 upon decreasing [CoTPPS] from 10 μM (S_{CO} = 82%) to 0.5 μM (S_{CO} = 41%).[35] We therefore directly compared the performance of our QD-CoTPPS system to that of the $[Ru(bpy)_3]^{2+}$-CoTPPS system using two different $[Ru(bpy)_3]^{2+}$ reaction mixtures. Both mixtures had the same concentration of the catalyst (0.25 μM CoTPPS) used in the QD system. System 1 had 12 μM $[Ru(bpy)_3]^{2+}$, which is the concentration that has the same absorbance as the QDs (2.5 μM) at the excitation wavelength for the reaction, 450 nm. System 2 used the optimized conditions of the benchmark report:[35] 500 μM of $[Ru(bpy)_3]^{2+}$ in an aqueous bicarbonate buffer. System 1 produced no CO and only a trace amount of H_2 (Table 1, entry 6 and Figure 2a). System 2 produced CO with a TON of 7,398 at the longest irradiation time of 72 h (Table 1, entry 7 and Figure 2a). Even given our optimization of the $[Ru(bpy)_3]^{2+}$ system, the TON for A-QD-CoTPPS is more than a factor of 10 higher than that of $[Ru(bpy)_3]^{2+}$-CoTPPS, even though the concentration of QDs is a factor of 200 lower than that of $[Ru(bpy)_3]^{2+}$. Furthermore, the QD systems produce CO with a selectivity of ∼99% for the entire illumination time (up to 96 h), while, for the $[Ru(bpy)_3]^{2+}$ system, the selectivity drops to 87.4% (Table 1, entry 7 and Figure 2b).

Figure 2c shows the sensitization efficiency, ξ—defined as the molecules of CO produced per J of absorbed photon energy—for the three QD-sensitized systems and the $[Ru(bpy)_3]^{2+}$-sensitized system. This parameter allows us to compare photocatalytic systems that use different excitation powers and illumination times, or, as in this case, different absorptivities of their sensitizers. ξ for the A-QDs is a factor of nearly 200 greater than ξ for $[Ru(bpy)_3]^{2+}$ when the concentration of CoTPPS is held constant (Table 1, entry 7), and ξ for the A-QDs is a factor of 10 greater than ξ for $[Ru(bpy)_3]^{2+}$ using the optimized conditions from the benchmark study.[35]

Origin of the High Catalytic Activity of the QD-CoTPPS System. In the nanoconfined environment of the QD surface, the pK_a of the terminal amine of aminoethanethiol (the ligand for the A-QDs) drops from ∼10 to ∼6 (see the

https://doi.org/10.1021/jacs.1c06961
J. Am. Chem. Soc. 2021, 143, 18131−18138

Table 1. Photocatalytic Performance for Various Sensitizers and Conditions[a]

Entry	CoTPPS (μM)	Sensitizer (μM)	Reaction conditions (mM)	Time (h)	TON		S_{CO} (%)	QY_{CO} (%)
					CO	H_2		
1	0.25	A-QDs (2.5)	NaAsc (25)	96	72,494	602	98.9	3.39
2	2.5	A-QDs (2.5)	NaAsc (25)	48	20,379	119	99.4	5.23
3	0.25	A-QDs (2.5)	NaAsc (5) + TCEP (5)	96	84,101	1,011	99.1	0.96
4	2.5	A-QDs (2.5)	NaAsc (5) + TCEP (5)	18	17,406	112	99.7	3.53
5	0.25	TMA-QDs (2.5)	NaAsc (25)	72	38,473	220	99.7	0.53
6	0.25	$[Ru(bpy)_3]^{2+}$ (12)	NaAsc (25)	72	–	16	–	–
7	0.25	$[Ru(bpy)_3]^{2+}$ (500)	NaAsc (100) + $NaHCO_3$ (100)	72	7,398	1,063	87.4	0.06[b]

[a]Summary of the reaction conditions used for the photocatalytic experiments. The pH measured before bubbling gas is 6.0–6.2 for entries 1–6 and 8.4 for entry 7. [b]The optimized QY reported in ref 35 is 0.81%. QYs are the average of three independent experiments. The uncertainty for TON values is ≤5%.

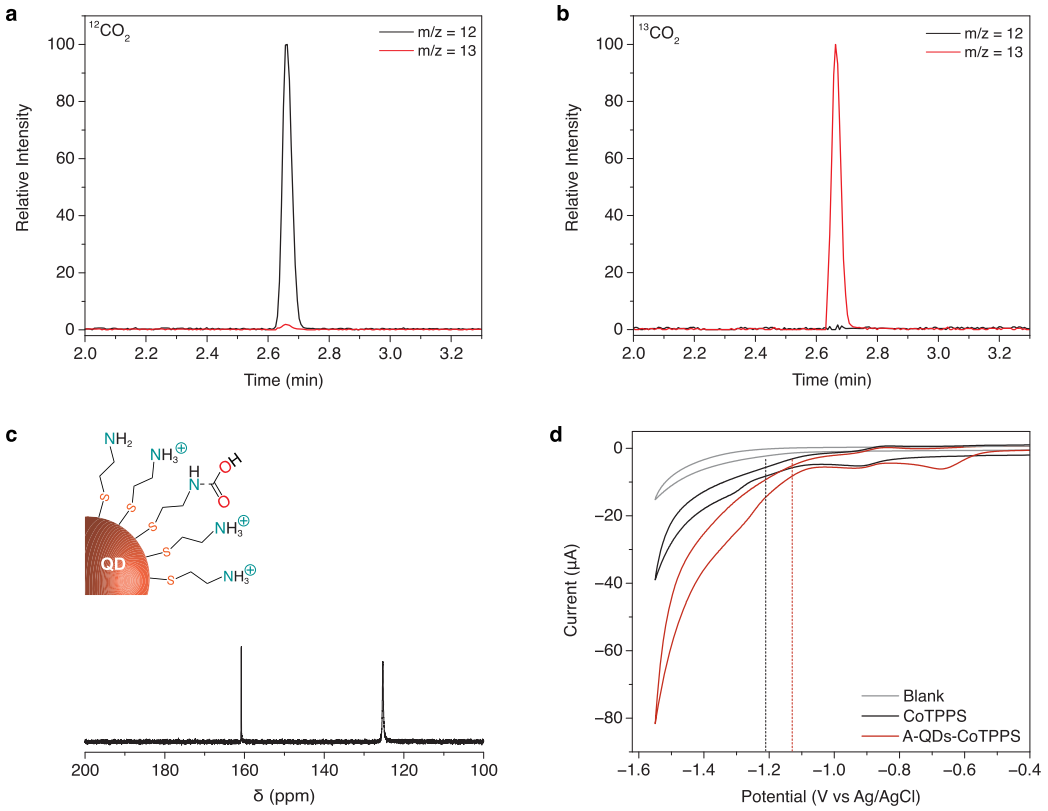

Figure 3. Isotope-labeled experiments and electrochemistry. (a,b) GC-MS chromatograms peaks (retention time of CO) with traces of m/z = 12 (black) and 13 (red) of the A-QDs-CoTPPS system in H_2O (pH 6.2) irradiated (450 nm) for 18 h and saturated with (a) CO_2 and (b) $^{13}CO_2$. (c) ^{13}C NMR spectrum of A-QDs in H_2O/D_2O (9:1 v/v) after exposure with $^{13}CO_2$. The measured pH before exposure was 6.1. The peak at 160.8 ppm is assigned to carbamic acid. The peak at 125.3 ppm is assigned to $^{13}CO_2$. (d) Cyclic voltammograms of CoTPPS with (red) and without (black) A-QDs in H_2O (pH 6.5) supported with 0.1 M KCl and saturated with CO_2. Scan rate was 50 mV·s^{-1}. The vertical dashed lines show the onset of catalytic current for CO_2 reduction potentials, determined from the intersection of the tangents between the baseline and the signal current.

Experimental Section in the SI). Consequently, only *ca.* 50% of the A-QD ligands have a terminal positive charge at the pH of our reaction mixture (6.0–6.2), while the remaining ligands of the A-QDs are present as free amines. While the decrease in positive charge of the A-QDs decreases the number of CoTPPS molecules that adsorb to their surfaces relative to the fully charged TMA-QDs in CO_2-purged water (Figure S8–9, SI), the TON of CO is nearly a factor of 2 higher for the A-QDs than for the TMA-QDs. These results show that the electrostatic assembly of sensitizer and catalyst is not the sole reason for the exceptional performance of the QD-CoTPPS system. We therefore examined the possible influence of the terminal amine of the A-QDs on this reaction.

The terminal amines of the A-QDs reversibly trap CO_2 as a carbamic acid precursor to CO. The ^{13}C NMR spectrum of an aqueous solution of A-QDs at pH 6.1 and bubbled with $^{13}CO_2$ shows a resonance at 160.8 ppm (Figure 3c), which coincides with resonances reported previously for carbamic acid formed upon complexation of CO_2 with amines, and a resonance at 125.3 ppm corresponding to dissolved CO_2.[55−57] The formation of the carbamic acid is consistent with the pK_a of the terminal amine of the A-QDs. If the pK_a of an amine is above ∼5, it will react with CO_2 at ambient pressure and

https://doi.org/10.1021/jacs.1c06961
J. Am. Chem. Soc. 2021, 143, 18131−18138

temperature in aqueous solution without promoters.[58] The amines on the A-QDs should therefore be capable of reacting with CO_2 under our conditions, but as *weakly basic* amines, i.e. amines basic enough to bond with CO_2 as a carbamic acid (with a weak N−C) bond, but not basic enough to form carbamate (with a strong N−C bond) at the pH of our reaction mixture.

Isotope labeled NMR experiments provide evidence of the lability of the N−C bond within the carbamic acid. The ^{13}C NMR spectrum of an aqueous solution of A-QDs at pH 6.1 bubbled with $^{13}CO_2$ shows the resonances of both ^{13}C-labeled carbamic acid and dissolved $^{13}CO_2$, but the amount and ratio of the two species depend on the degree to which the sample has been degassed by FPT or purging with He. An array of experiments detailed in the Supporting Information (SI) (Figure S10, SI) show that (i) FPT removes all CO_2 from the system, even the CO_2 bound as carbamic acid,[57] (ii) the formation of carbamic acid is reversible under mild conditions in our system, and (iii) purging the sample with He removes more freely diffusing CO_2 than carbamic acid. Clearly, the amine does "trap" the CO_2, but with a labile bond.

Interestingly, the A-QD-CoTPPS system efficiently reduces low concentrations of CO_2 to CO (75−10 vol %, Ar balanced) and produces a small amount of CO (TON = 3852) even when exposed to air and then purged with Ar instead of CO_2, but does not produce CO when subjected to freeze−pump−thaw cycles before purging with Ar (Table S2, SI). The latter result suggests that the amines on the QD surface may also be suitable for direct capture of CO_2 from air, as has been recently reported by Long and co-workers for tetraamine-appended metal−organic frameworks,[47] and that the resulting carbamic acids can serve as precursors to CO. This conclusion is supported by experiments where we produce ^{13}CO from samples from which we have purged with $^{13}CO_2$ but then evacuated the headspace before illumination (Figure S11, SI). The detection of $^{13}CO_2$ in the headspace of these samples after 18 h of illumination further support the existence of a dynamic equilibrium between all three forms/phases of CO_2.

From these experiments, we propose that this sequestration of CO_2 as a carbamic acid gives the A-QDs an advantage over the TMA-QDs, and over the $[Ru(bpy)_3]^{2+}$ system, in the photocatalytic reduction of CO_2 to CO. The dynamic equilibrium of the carbamic acid with free CO_2 dissolved and in the headspace allows the carbamic acid to serve as a regenerable reaction intermediate, a catalyst-proximate reservoir for CO_2, and a direct or indirect precursor to the CO_2-bound porphyrin. This function is especially important in a pure (non buffered) water system because it effectively increases the solubility of CO_2. A similar strategy is employed in catalytic hydrogenations of CO_2 to MeOH, where ammonium carbamate is used as a CO_2 source for MeOH,[59,60] but only at elevated temperatures. Since the N−C bond of our carbamic acid precursor is much weaker than that of the carbamate bond, we do not need elevated temperatures or other stimuli to utilize it as a precursor.

The A-QDs lower the onset potential for catalytic CO_2 reduction. We find direct evidence for the promotion of CO_2 reduction by the sequestration of CO_2 as carbamic acid in the electrochemical response of CoTPPS in the absence or presence of the two types of QDs or their respective free ligands (Figure 3d and Figure S12, SI). The cyclic voltammetry (CV) for CoTPPS recorded in a CO_2-saturated aqueous solution (pH 6.5 before CO_2 purging, supported with 0.1 M KCl) shows two redox events corresponding to $Co^{II}TPPS/[Co^{I}(TPPS)]^{-}$ and $[Co^{I}(TPPS)]^{-}/[Co^{I}(TPPS^{\bullet-})]^{2-}$ (Figure 3d, black).[35] While there is no significant change at the first reduction wave under CO_2 vs Ar (Figure S12, SI), the formation of the reduced porphyrin intermediate $[Co^{I}(TPPS^{\bullet-})]^{2-}$ is coupled with the rise of catalytic current in a CO_2 atmosphere. This result is consistent with the published catalytic cycle for CoTPPS,[35] which indicates that $[Co^{I}(TPPS^{\bullet-})]^{2-}$ is the species to which CO_2 binds affording $[Co^{III}(TPPS^{\bullet-})(CO_2^{2-})]^{2-}$, which is then protonated to $[Co^{III}(TPPS^{\bullet-})(CO_2H^{-})]^{-}$. Subsequent steps of C−O bond cleavage coupled with protonation and water elimination regenerate the initial form of the catalyst.

Figure 3d shows that the onset potential for catalytic CO_2 reduction shifts anodically by 80 mV, from −1.21 V for CoTPPS to −1.13 V vs Ag/AgCl for A-QDs-CoTPPS, but that no meaningful changes in this potential occur upon addition of TMA-QDs, or 2-aminoethanethiol (AET) or 2- mercaptoethyl-*N*,*N*,*N*-trimethylammonium (TMA) ligands without QDs (Figure S12, SI). This result confirms that it is the presence of QD-bound carbamic acid (the species present in samples of A-QDs bubbled with CO_2) that enables this reduction in onset potential for catalysis. A peak at ca. −0.6 V vs Ag/AgCl is possibly attributable to ligand-coordinated CoTPPS at the high concentrations used for recording the CVs,[61,62] but photocatalytic experiments using the $[Ru(bpy)_3]^{2+}$-CoTPPS system with TMA or AET added in the relevant concentrations confirms that the ligands alone (without QDs) have no beneficial effect on the photocatalysis, whether or not they coordinate the porphyrin (Table S3, SI).

We suspect, but have not proven, that the A-QDs decrease the onset potential for catalysis through (i) an increase in the local proton concentration that facilitates the protonation step of the catalytic cycle or (ii) hydrogen bonding interactions between the NH fragments of the carbamic acid and the CO_2 adduct coordinated to the metal center, which stabilize the latter and assist in C−O bond cleavage. Such "second-sphere" effects on the activation and transformation of CO_2 have been accomplished by, for example, the phenol-based pendants on iron tetraphenylporphyrins by Savéant, Costentin and Robert and co-workers,[63,64] the amide or urea arms on iron tetraphenylporphyrins reported by Chang and co-workers or Aukauloo and co-workers,[65,66] and the iron hangman porphyrin with a guanidinium group reported by Nocera and co-workers.[67]

CONCLUSIONS

We have reported a simple three-component photocatalytic system for CO_2 reduction to CO in pure water. The system comprises a $CuInS_2$ QD sensitizer and cobalt porphyrin catalyst and operates with unprecedented turnover number (>80,000), and an unprecedented combination of TON, quantum yield (5.2%), sensitization efficiency (95.8 mol CO/J photon energy absorbed), and selectivity (>99%) (Table S1, SI). The amine/ammonium-terminated ligand shells of the QDs are responsible for the exceptional performance of this system. These values greatly exceed the TON (926), quantum yield (0.81%), sensitization efficiency (9.3), and selectivity (82%), achieved by the benchmark system: a $[Ru(bpy)_3]^{2+}$ photosensitizer with the same Co-porphyrin catalyst, even when the concentration of the $[Ru(bpy)_3]^{2+}$ is a factor 200 higher than that of the QDs. We cannot trace the trajectory of a single CO_2 molecule, or prove that our carbamic acid binds

https://doi.org/10.1021/jacs.1c06961
J. Am. Chem. Soc. 2021, 143, 18131−18138

to the cobalt center,[68] but our results prove that the amine/ammonium-terminated ligand shells of the QDs enhance the catalysis by establishing (i) an electrostatic assembly with CoTPPS, which allow the colocalization of protons, CO_2, and catalyst at the QD core that serves at the source of the electrons; (ii) a dynamic equilibrium between carbamic acid and free CO_2 that increases the local concentration of available CO_2; and (iii) "second-sphere" effects that improve the efficiency of the CoTPPS catalyst. Our room-temperature capture−conversion approach is possible because of the nanoconfined environment of the QD surface, which enables the particular reactivity of the carbamic acid as a labile sequestration agent. This reactivity is specified by the electrostatic environment at the QD surface, which itself is tunable through manipulation of the structure and density of the QDs' ligands.

The A-QD-CoTPPS system reported here is currently limited by the use of sodium ascorbate as a sacrificial reagent and the accumulation of its oxidized form, DHA, which decreases the colloidal stability of the QDs and prevents their indefinite operation. We anticipate this stability issue can be addressed with either a flow cell system or by preparing the QDs as a porous material or hydrogel system.[69,70]

The importance of these results lies in the QD system's exceptional performance in water, which allows its future incorporation into devices that supply protons and reductive equivalents for CO_2 reduction with a water splitting reaction, potentially through a Z-scheme.[71] Adaptation of this system for that purpose requires the use of more oxidative nanocrystals, but, if it can be achieved, it is feasible that we use this system to produce CO within a photochemical cascade to achieve artificial photosynthesis of liquid fuels.[72] Future advances might also require modification of the peripherical groups on the cobalt porphyrin catalyst, for example to bind it to a photoelectrode; our preliminary photocatalytic output from a tetracarboxyphenyl cobalt porphyrin photosensitized by QDs is promising (TON_{CO} = 28,282, Figure S13, SI) and supports the feasibility of such advances. Notably, our current optimized system operates in unbuffered pure water, whereas the current high-performing molecule-sensitized systems require either alkaline pH or additives that serve as buffers,[35,38] thus limiting their potential for larger scale CO production.

■ ASSOCIATED CONTENT

Supporting Information

The Supporting Information is available free of charge at https://pubs.acs.org/doi/10.1021/jacs.1c06961.

Supplementary tables containing literature data, additional details about materials and synthesis, QDs characterization, photocatalytic reactions and performances, chromatographic detection of gases, NMR characterization, measurement of QYs, TON, TOF, and sensitization efficiencies, and electrochemical characterization (PDF)

■ AUTHOR INFORMATION

Corresponding Author

Emily A. Weiss − *Department of Chemistry and Department of Materials Science and Engineering, Northwestern University, Evanston, Illinois 60208, United States; Center for Bio-Inspired Energy Science, Northwestern University, Chicago, Illinois 60611, United States;* orcid.org/0000-0001-5834-463X; Email: e-weiss@northwestern.edu

Authors

Francesca Arcudi − *Department of Chemistry, Northwestern University, Evanston, Illinois 60208, United States; Center for Bio-Inspired Energy Science, Northwestern University, Chicago, Illinois 60611, United States;* orcid.org/0000-0003-1909-5241

Luka Đorđević − *Department of Chemistry, Northwestern University, Evanston, Illinois 60208, United States; Center for Bio-Inspired Energy Science, Northwestern University, Chicago, Illinois 60611, United States;* orcid.org/0000-0002-8346-7110

Benjamin Nagasing − *Department of Chemistry, Northwestern University, Evanston, Illinois 60208, United States*

Samuel I. Stupp − *Department of Chemistry, Department of Materials Science and Engineering, and Department of Biomedical Engineering, Northwestern University, Evanston, Illinois 60208, United States; Center for Bio-Inspired Energy Science, Department of Medicine, and Simpson Querrey Institute, Northwestern University, Chicago, Illinois 60611, United States;* orcid.org/0000-0002-5491-7442

Complete contact information is available at: https://pubs.acs.org/10.1021/jacs.1c06961

Author Contributions

¶F.A. and L.Đ. contributed equally to this work.

Notes

The authors declare the following competing financial interest(s): The authors are coinventors on a provisional patent application entitled "Quantum Dot Sensitized Photoreduction of Carbon Dioxide" related to his work.

■ ACKNOWLEDGMENTS

This work was supported as part of the Center for Bio-Inspired Energy Science (CBES), an Energy Frontier Research Center (EFRC) funded by the US Department of Energy, Office of Science, Basic Energy Sciences under Award No. DE-SC0000989. This work made use of the IMSERC at Northwestern University, which has received support from the NIH (1S10OD012016-01/1S10RR019071-01A1); the Soft and Hybrid Nanotechnology Experimental (SHyNE) Resource (NSF ECCS-1542205); the State of Illinois and the International Institute for Nanotechnology (IIN); and the REACT Core facility, which acknowledges funding from the U.S. Department of Energy, Catalysis Science program (DE-SC0001329) for the purchase of the GC-MS system. We thank Prof. Neil Schweitzer and Dr. Selim Alayoglu for facilitating instrument use in REACT.

■ REFERENCES

(1) Lewis, N. S.; Nocera, D. G. Powering the Planet: Chemical Challenges in Solar Energy Utilization. *Proc. Natl. Acad. Sci. U. S. A.* **2006**, *103*, 15729−15735.

(2) Creutzig, F.; Agoston, P.; Goldschmidt, J. C.; Luderer, G.; Nemet, G.; Pietzcker, R. C. The Underestimated Potential of Solar Energy to Mitigate Climate Change. *Nat. Energy* **2017**, *2*, 17140.

(3) Zimmerman, J. B.; Anastas, P. T.; Erythropel, H. C.; Leitner, W. Designing for a Green Chemistry Future. *Science* **2020**, *367*, 397−400.

(4) Jiang, Z.; Sun, H.; Wang, T.; Wang, B.; Wei, W.; Li, H.; Yuan, S.; An, T.; Zhao, H.; Yu, J.; Wong, P. K. Nature-Based Catalyst for

Visible-Light-Driven Photocatalytic CO_2 Reduction. *Energy Environ. Sci.* **2018**, *11*, 2382−2389.
(5) Kondratenko, E. V.; Mul, G.; Baltrusaitis, J.; Larrazábal, G. O.; Pérez-Ramírez, J. Status and Perspectives of CO_2 Conversion into Fuels and Chemicals by Catalytic, Photocatalytic and Electrocatalytic Processes. *Energy Environ. Sci.* **2013**, *6*, 3112−3135.
(6) Huang, J.; Hörmann, N.; Oveisi, E.; Loiudice, A.; De Gregorio, G. L.; Andreussi, O.; Marzari, N.; Buonsanti, R. Potential-Induced Nanoclustering of Metallic Catalysts during Electrochemical CO_2 Reduction. *Nat. Commun.* **2018**, *9*, 3117.
(7) Kosco, J.; Bidwell, M.; Cha, H.; Martin, T.; Howells, C. T.; Sachs, M.; Anjum, D. H.; Gonzalez Lopez, S.; Zou, L.; Wadsworth, A.; Zhang, W.; Zhang, L.; Tellam, J.; Sougrat, R.; Laquai, F.; DeLongchamp, D. M.; Durrant, J. R.; McCulloch, I. Enhanced Photocatalytic Hydrogen Evolution from Organic Semiconductor Heterojunction Nanoparticles. *Nat. Mater.* **2020**, *19*, 559−565.
(8) Takata, T.; Jiang, J.; Sakata, Y.; Nakabayashi, M.; Shibata, N.; Nandal, V.; Seki, K.; Hisatomi, T.; Domen, K. Photocatalytic Water Splitting with a Quantum Efficiency of Almost Unity. *Nature* **2020**, *581*, 411−414.
(9) Lennox, J. C.; Kurtz, D. A.; Huang, T.; Dempsey, J. L. Excited-State Proton-Coupled Electron Transfer: Different Avenues for Promoting Proton/Electron Movement with Solar Photons. *ACS Energy Lett.* **2017**, *2*, 1246−1256.
(10) Lee, K. J.; Elgrishi, N.; Kandemir, B.; Dempsey, J. L. Electrochemical and Spectroscopic Methods for Evaluating Molecular Electrocatalysts. *Nat. Rev. Chem.* **2017**, *1*, 0039.
(11) Banin, U.; Waiskopf, N.; Hammarström, L.; Boschloo, G.; Freitag, M.; Johansson, E. M. J.; Sá, J.; Tian, H.; Johnston, M. B.; Herz, L. M.; Milot, R. L.; Kanatzidis, M. G.; Ke, W.; Spanopoulos, I.; Kohlstedt, K. L.; Schatz, G. C.; Lewis, N.; Meyer, T.; Nozik, A. J.; et al. Nanotechnology for Catalysis and Solar Energy Conversion. *Nanotechnology* **2021**, *32*, 042003.
(12) Young, K. J.; Martini, L. A.; Milot, R. L.; Snoeberger, R. C.; Batista, V. S.; Schmuttenmaer, C. A.; Crabtree, R. H.; Brudvig, G. W. Light-Driven Water Oxidation for Solar Fuels. *Coord. Chem. Rev.* **2012**, *256*, 2503−2520.
(13) Han, Z.; Qiu, F.; Eisenberg, R.; Holland, P. L.; Krauss, T. D. Robust Photogeneration of H_2 in Water Using Semiconductor Nanocrystals and a Nickel Catalyst. *Science* **2012**, *338*, 1321−1324.
(14) Ceballos, B. M.; Yang, J. Y. Directing the Reactivity of Metal Hydrides for Selective CO_2 Reduction. *Proc. Natl. Acad. Sci. U. S. A.* **2018**, *115*, 12686−12691.
(15) Barlow, J. M.; Yang, J. Y. Thermodynamic Considerations for Optimizing Selective CO_2 Reduction by Molecular Catalysts. *ACS Cent. Sci.* **2019**, *5*, 580−588.
(16) Burke, R.; Bren, K. L.; Krauss, T. D. Semiconductor Nanocrystal Photocatalysis for the Production of Solar Fuels. *J. Chem. Phys.* **2021**, *154*, 030901.
(17) Bushuyev, O. S.; De Luna, P.; Dinh, C. T.; Tao, L.; Saur, G.; van de Lagemaat, J.; Kelley, S. O.; Sargent, E. H. What Should We Make with CO_2 and How Can We Make It? *Joule* **2018**, *2*, 825−832.
(18) Dong, Y.; Duchesne, P.; Mohan, A.; Ghuman, K. K.; Kant, P.; Hurtado, L.; Ulmer, U.; Loh, J. Y. Y.; Tountas, A. A.; Wang, L.; Jelle, A.; Xia, M.; Dittmeyer, R.; Ozin, G. A. Shining Light on CO_2: From Materials Discovery to Photocatalyst, Photoreactor and Process Engineering. *Chem. Soc. Rev.* **2020**, *49*, 5648−5663.
(19) He, J.; Janáky, C. Recent Advances in Solar-Driven Carbon Dioxide Conversion: Expectations versus Reality. *ACS Energy Lett.* **2020**, *5*, 1996−2014.
(20) Wu, J.; Huang, Y.; Ye, W.; Li, Y. CO_2 Reduction: From the Electrochemical to Photochemical Approach. *Adv. Sci.* **2017**, *4*, 1700194.
(21) Smith, P. T.; Nichols, E. M.; Cao, Z.; Chang, C. J. Hybrid Catalysts for Artificial Photosynthesis: Merging Approaches from Molecular, Materials, and Biological Catalysis. *Acc. Chem. Res.* **2020**, *53*, 575−587.
(22) Guo, Z.; Cheng, S.; Cometto, C.; Anxolabéhère-Mallart, E.; Ng, S.-M.; Ko, C.-C.; Liu, G.; Chen, L.; Robert, M.; Lau, T.-C. Highly Efficient and Selective Photocatalytic CO_2 Reduction by Iron and Cobalt Quaterpyridine Complexes. *J. Am. Chem. Soc.* **2016**, *138*, 9413−9416.
(23) Ma, B.; Chen, G.; Fave, C.; Chen, L.; Kuriki, R.; Maeda, K.; Ishitani, O.; Lau, T. C.; Bonin, J.; Robert, M. Efficient Visible-Light-Driven CO_2 Reduction by a Cobalt Molecular Catalyst Covalently Linked to Mesoporous Carbon Nitride. *J. Am. Chem. Soc.* **2020**, *142*, 6188−6195.
(24) Ouyang, T.; Wang, H.-J.; Huang, H.-H.; Wang, J.-W.; Guo, S.; Liu, W.-J.; Zhong, D.-C.; Lu, T.-B. Dinuclear Metal Synergistic Catalysis Boosts Photochemical CO_2-to-CO Conversion. *Angew. Chem., Int. Ed.* **2018**, *57*, 16480−16485.
(25) Thoi, V. S.; Kornienko, N.; Margarit, C. G.; Yang, P.; Chang, C. J. Visible-Light Photoredox Catalysis: Selective Reduction of Carbon Dioxide to Carbon Monoxide by a Nickel *N*-Heterocyclic Carbene−Isoquinoline Complex. *J. Am. Chem. Soc.* **2013**, *135*, 14413−14424.
(26) Kuramochi, Y.; Kamiya, M.; Ishida, H. Photocatalytic CO_2 Reduction in N,N-Dimethylacetamide/Water as an Alternative Solvent System. *Inorg. Chem.* **2014**, *53*, 3326−3332.
(27) Cancelliere, A. M.; Puntoriero, F.; Serroni, S.; Campagna, S.; Tamaki, Y.; Saito, D.; Ishitani, O. Efficient Trinuclear Ru(II)−Re(I) Supramolecular Photocatalysts for CO_2 Reduction Based on a New Tris-Chelating Bridging Ligand Built around a Central Aromatic Ring. *Chem. Sci.* **2020**, *11*, 1556−1563.
(28) Costentin, C.; Robert, M.; Savéant, J.-M. Catalysis of the Electrochemical Reduction of Carbon Dioxide. *Chem. Soc. Rev.* **2013**, *42*, 2423−2436.
(29) Lide, D. R. *Handbook of Chemistry and Physics*, 81st ed.; CRC: Boca Raton, FL, 2000.
(30) Karmakar, S.; Barman, S.; Rahimi, F. A.; Maji, T. K. Covalent Grafting of Molecular Photosensitizer and Catalyst on MOF-808: Effect of Pore Confinement toward Visible Light-Driven CO_2 Reduction in Water. *Energy Environ. Sci.* **2021**, *14*, 2429−2440.
(31) Bi, Q.-Q.; Wang, J.-W.; Lv, J.-X.; Wang, J.; Zhang, W.; Lu, T.-B. Selective Photocatalytic CO_2 Reduction in Water by Electrostatic Assembly of CdS Nanocrystals with a Dinuclear Cobalt Catalyst. *ACS Catal.* **2018**, *8*, 11815−11821.
(32) Kuehnel, M. F.; Orchard, K. L.; Dalle, K. E.; Reisner, E. Selective Photocatalytic CO_2 Reduction in Water through Anchoring of a Molecular Ni Catalyst on CdS Nanocrystals. *J. Am. Chem. Soc.* **2017**, *139*, 7217−7223.
(33) Nakada, A.; Koike, K.; Maeda, K.; Ishitani, O. Highly Efficient Visible-Light-Driven CO_2 Reduction to CO Using a Ru(II)−Re(I) Supramolecular Photocatalyst in an Aqueous Solution. *Green Chem.* **2016**, *18*, 139−143.
(34) Chaudhary, Y. S.; Woolerton, T. W.; Allen, C. S.; Warner, J. H.; Pierce, E.; Ragsdale, S. W.; Armstrong, F. A. Visible Light-Driven CO_2 Reduction by Enzyme Coupled CdS Nanocrystals. *Chem. Commun.* **2012**, *48*, 58−60.
(35) Call, A.; Cibian, M.; Yamamoto, K.; Nakazono, T.; Yamauchi, K.; Sakai, K. Highly Efficient and Selective Photocatalytic CO_2 Reduction to CO in Water by a Cobalt Porphyrin Molecular Catalyst. *ACS Catal.* **2019**, *9*, 4867−4874.
(36) Pitman, C. L.; Brereton, K. R.; Miller, A. J. M. Aqueous Hydricity of Late Metal Catalysts as a Continuum Tuned by Ligands and the Medium. *J. Am. Chem. Soc.* **2016**, *138*, 2252−2260.
(37) Rohacova, J.; Ishitani, O. Rhenium(I) Trinuclear Rings as Highly Efficient Redox Photosensitizers for Photocatalytic CO_2 Reduction. *Chem. Sci.* **2016**, *7*, 6728−6739.
(38) Nakada, A.; Koike, K.; Maeda, K.; Ishitani, O. Highly Efficient Visible-Light-Driven CO_2 Reduction to CO Using a Ru(II)-Re(I) Supramolecular Photocatalyst in an Aqueous Solution. *Green Chem.* **2016**, *18*, 139−143.
(39) Lian, S.; Kodaimati, M. S.; Dolzhnikov, D. S.; Calzada, R.; Weiss, E. A. Powering a CO_2 Reduction Catalyst with Visible Light through Multiple Sub-Picosecond Electron Transfers from a Quantum Dot. *J. Am. Chem. Soc.* **2017**, *139*, 8931−8938.

https://doi.org/10.1021/jacs.1c06961
J. Am. Chem. Soc. 2021, 143, 18131−18138

(40) Perez, K. A.; Rogers, C. R.; Weiss, E. A. Quantum Dot-Catalyzed Photoreductive Removal of Sulfonyl-Based Protecting Groups. *Angew. Chem., Int. Ed.* **2020**, *59*, 14091−14095.
(41) Lian, S.; Kodaimati, M. S.; Weiss, E. A. Photocatalytically Active Superstructures of Quantum Dots and Iron Porphyrins for Reduction of CO_2 to CO in Water. *ACS Nano* **2018**, *12*, 568−575.
(42) Pankhurst, J. R.; Guntern, Y. T.; Mensi, M.; Buonsanti, R. Molecular Tunability of Surface-Functionalized Metal Nanocrystals for Selective Electrochemical CO_2 Reduction. *Chem. Sci.* **2019**, *10*, 10356−10365.
(43) Meng, N.; Liu, C.; Liu, Y.; Yu, Y.; Zhang, B. Efficient Electrosynthesis of Syngas with Tunable CO/H_2 Ratios over $Zn_xCd_{1-x}S$-Amine Inorganic−Organic Hybrids. *Angew. Chem., Int. Ed.* **2019**, *58*, 18908−18912.
(44) Cho, K. M.; Kim, K. H.; Park, K.; Kim, C.; Kim, S.; Al-Saggaf, A.; Gereige, I.; Jung, H.-T. Amine-Functionalized Graphene/CdS Composite for Photocatalytic Reduction of CO_2. *ACS Catal.* **2017**, *7*, 7064−7069.
(45) Wagner, A.; Sahm, C. D.; Reisner, E. Towards Molecular Understanding of Local Chemical Environment Effects in Electro- and Photocatalytic CO_2 Reduction. *Nat. Catal.* **2020**, *3*, 775−786.
(46) McDonald, T. M.; Mason, J. A.; Kong, X.; Bloch, E. D.; Gygi, D.; Dani, A.; Crocellà, V.; Giordanino, F.; Odoh, S. O.; Drisdell, W. S.; Vlaisavljevich, B.; Dzubak, A. L.; Poloni, R.; Schnell, S. K.; Planas, N.; Lee, K.; Pascal, T.; Wan, L. F.; Prendergast, D.; et al. Cooperative Insertion of CO_2 in Diamine-Appended Metal-Organic Frameworks. *Nature* **2015**, *519*, 303−308.
(47) Kim, E. J.; Siegelman, R. L.; Jiang, H. Z. H.; Forse, A. C.; Lee, J. H.; Martell, J. D.; Milner, P. J.; Falkowski, J. M.; Neaton, J. B.; Reimer, J. A.; Weston, S. C.; Long, J. R. Cooperative Carbon Capture and Steam Regeneration with Tetraamine-Appended Metal-Organic Frameworks. *Science* **2020**, *369*, 392−396.
(48) Rochelle, G. T. Amine Scrubbing for CO_2 Capture. *Science* **2009**, *325*, 1652−1654.
(49) Chang, X.; Wang, T.; Gong, J. CO_2 Photo-Reduction: Insights into CO_2 Activation and Reaction on Surfaces of Photocatalysts. *Energy Environ. Sci.* **2016**, *9*, 2177−2196.
(50) Liu, H.; Chu, J.; Yin, Z.; Cai, X.; Zhuang, L.; Deng, H. Covalent Organic Frameworks Linked by Amine Bonding for Concerted Electrochemical Reduction of CO_2. *Chem.* **2018**, *4*, 1696−1709.
(51) Zhang, X.; Yamauchi, K.; Sakai, K. Earth-Abundant Photocatalytic CO_2 Reduction by Multielectron Chargeable Cobalt Porphyrin Catalysts: High CO/H_2 Selectivity in Water Based on Phase Mismatch in Frontier MO Association. *ACS Catal.* **2021**, *11*, 10436−10449.
(52) Martindale, B. C. M.; Joliat, E.; Bachmann, C.; Alberto, R.; Reisner, E. Clean Donor Oxidation Enhances the H_2 Evolution Activity of a Carbon Quantum Dot−Molecular Catalyst Photosystem. *Angew. Chem., Int. Ed.* **2016**, *55*, 9402−9406.
(53) Li, X.-B.; Li, Z.-J.; Gao, Y.-J.; Meng, Q.-Y.; Yu, S.; Weiss, R. G.; Tung, C.-H.; Wu, L.-Z. Mechanistic Insights into the Interface-Directed Transformation of Thiols into Disulfides and Molecular Hydrogen by Visible-Light Irradiation of Quantum Dots. *Angew. Chem.* **2014**, *126*, 2117−2121.
(54) Boutin, E.; Robert, M. Molecular Electrochemical Reduction of CO_2 beyond Two Electrons. *Trends Chem.* **2021**, *3*, 359−372.
(55) Kortunov, P. V.; Siskin, M.; Baugh, L. S.; Calabro, D. C. In Situ Nuclear Magnetic Resonance Mechanistic Studies of Carbon Dioxide Reactions with Liquid Amines in Aqueous Systems: New Insights on Carbon Capture Reaction Pathways. *Energy Fuels* **2015**, *29*, 5919−5939.
(56) Bhattacharyya, S.; Shah, F. U. Ether Functionalized Choline Tethered Amino Acid Ionic Liquids for Enhanced CO_2 Capture. *ACS Sustainable Chem. Eng.* **2016**, *4*, 5441−5449.
(57) Pinto, M. L.; Mafra, L.; Guil, J. M.; Pires, J.; Rocha, J. Adsorption and Activation of CO_2 by Amine-Modified Nanoporous Materials Studied by Solid-State NMR and $^{13}CO_2$ Adsorption. *Chem. Mater.* **2011**, *23*, 1387−1395.
(58) Kortunov, P. V.; Siskin, M.; Baugh, L. S.; Calabro, D. C. In Situ Nuclear Magnetic Resonance Mechanistic Studies of Carbon Dioxide Reactions with Liquid Amines in Aqueous Systems: New Insights on Carbon Capture Reaction Pathways. *Energy Fuels* **2015**, *29*, 5919−5939.
(59) Rezayee, N. M.; Huff, C. A.; Sanford, M. S. Tandem Amine and Ruthenium-Catalyzed Hydrogenation of CO_2 to Methanol. *J. Am. Chem. Soc.* **2015**, *137*, 1028−1031.
(60) Mathis, C. L.; Geary, J.; Ardon, Y.; Reese, M. S.; Philliber, M. A.; VanderLinden, R. T.; Saouma, C. T. Thermodynamic Analysis of Metal−Ligand Cooperativity of PNP Ru Complexes: Implications for CO_2 Hydrogenation to Methanol and Catalyst Inhibition. *J. Am. Chem. Soc.* **2019**, *141*, 14317−14328.
(61) Jiang, F.; Siegler, M. A.; Sun, X.; Jiang, L.; Fonseca Guerra, C.; Bouwman, E. Redox Interconversion between Cobalt(III) Thiolate and Cobalt(II) Disulfide Compounds. *Inorg. Chem.* **2018**, *57*, 8796−8805.
(62) Dey, S.; Todorova, T. K.; Fontecave, M.; Mougel, V. Electroreduction of CO_2 to Formate with Low Overpotential Using Cobalt Pyridine Thiolate Complexes. *Angew. Chem., Int. Ed.* **2020**, *59*, 15726−15733.
(63) Costentin, C.; Drouet, S.; Robert, M.; Savéant, J.-M. A Local Proton Source Enhances CO_2 Electroreduction to CO by a Molecular Fe Catalyst. *Science* **2012**, *338*, 90−94.
(64) Costentin, C.; Passard, G.; Robert, M.; Savéant, J. M. Ultraefficient Homogeneous Catalyst for the CO_2-to-CO Electrochemical Conversion. *Proc. Natl. Acad. Sci. U. S. A.* **2014**, *111*, 14990−14994.
(65) Nichols, E. M.; Derrick, J. S.; Nistanaki, S. K.; Smith, P. T.; Chang, C. J. Positional Effects of Second-Sphere Amide Pendants on Electrochemical CO_2 Reduction Catalyzed by Iron Porphyrins. *Chem. Sci.* **2018**, *9*, 2952−2960.
(66) Gotico, P.; Boitrel, B.; Guillot, R.; Sircoglou, M.; Quaranta, A.; Halime, Z.; Leibl, W.; Aukauloo, A. Second-Sphere Biomimetic Multipoint Hydrogen-Bonding Patterns to Boost CO_2 Reduction of Iron Porphyrins. *Angew. Chem., Int. Ed.* **2019**, *58*, 4504−4509.
(67) Margarit, C. G.; Schnedermann, C.; Asimow, N. G.; Nocera, D. G. Carbon Dioxide Reduction by Iron Hangman Porphyrins. *Organometallics* **2019**, *38*, 1219−1223.
(68) Nakajima, T.; Tamaki, Y.; Ueno, K.; Kato, E.; Nishikawa, T.; Ohkubo, K.; Yamazaki, Y.; Morimoto, T.; Ishitani, O. Photocatalytic Reduction of Low Concentration of CO_2. *J. Am. Chem. Soc.* **2016**, *138*, 13818−13821.
(69) Mohanan, J. L.; Arachchige, I. U.; Brock, S. L. Porous Semiconductor Chalcogenide Aerogels. *Science* **2005**, *307*, 397−400.
(70) Weingarten, A. S.; Kazantsev, R. V.; Palmer, L. C.; McClendon, M.; Koltonow, A. R.; Samuel, A. P. S.; Kiebala, D. J.; Wasielewski, M. R.; Stupp, S. I. Self-Assembling Hydrogel Scaffolds for Photocatalytic Hydrogen Production. *Nat. Chem.* **2014**, *6*, 964−970.
(71) Wang, Q.; Warnan, J.; Rodríguez-Jiménez, S.; Leung, J. J.; Kalathil, S.; Andrei, V.; Domen, K.; Reisner, E. Molecularly Engineered Photocatalyst Sheet for Scalable Solar Formate Production from Carbon Dioxide and Water. *Nat. Energy* **2020**, *5*, 703−710.
(72) Gadiyar, C.; Loiudice, A.; Buonsanti, R. Colloidal Nanocrystals for Photoelectrochemical and Photocatalytic Water Splitting. *J. Phys. D: Appl. Phys.* **2017**, *50*, 074006.

https://doi.org/10.1021/jacs.1c06961
J. Am. Chem. Soc. 2021, 143, 18131−18138